Astronomy & Astrophysics manuscript no. aa_letter
March 24, 2026

A quasi-star is born: formation and evolution of accreting quasi-stars as a metallicity-independent pathway to Little Red Dots

J. Roman-Garza[1,2,⋆], D. Schaerer[1,3], C. Charbonnel[1,3], T. Fragos[1,2], E. Cenci[1], R. Marques-Chaves[1], P. A. Oesch[1,4], and M. Xiao[1]

[1] Département d'Astronomie, Université de Genève, Chemin Pegasi 51, CH-1290 Versoix, Switzerland
[2] Gravitational Wave Science Center (GWSC), Université de Genève, CH-1211 Geneva, Switzerland.
[3] CNRS, IRAP, 14 Avenue E. Belin, 31400 Toulouse, France
[4] Cosmic Dawn Center (DAWN), Niels Bohr Institute, University of Copenhagen, Jagtvej 128, København N, DK-2200, Denmark

Received date; Accepted date

ABSTRACT

To investigate the rest-frame optical emission of "Little Red Dots", we model the formation of and evolution of quasi-stars, i.e. stellar envelopes supported by the accretion luminosity onto a central black hole, originating from rapidly accreting proto-stars reaching the supermassive star regime ($> 10^4$ M$_\odot$) and undergoing general relativistic instability. We compute stellar evolution models with net mass gain rates = 0.01, 0.1, and 1 M$_\odot$/yr and metallicities Z = 0–0.01. For the mass gain rates $\geq$ 0.1 M$_\odot$/yr, stars remain nearly fully convective with $T_{\rm eff} \sim$ 4000–9000 K. The general relativistic instability leading to central BH formation occurs at $M_\star \sim 3.5 \times 10^4$ M$_\odot$ (6.6×10^4 M$_\odot$) for $\dot{M}_{\rm acc}$ = 0.1 M$_\odot$/yr (1 M$_\odot$/yr), at luminosities $L \sim 10^9$ L$_\odot$. The lifetime of quasi-stars is estimated to be 10^7–10^8 yr, ~100–1000 times longer than their progenitors. In an environment allowing for rapid accretion the formation, evolution, and properties of quasi-stars are found be essentially independent of metallicity. Comparing the luminosities of our models with those of Little Red Dots at $z < 4.5$ ($L_{\rm bol} \sim 10^{9.5}$–$10^{11.5}$ L$_\odot$) yields quasi-star masses $10^{4.5}$–$10^{6.5}$ M$_\odot$. The observed minimum luminosity of $\sim 10^{9.5}$ L$_\odot$ implies accretion rates $\gtrsim$ 0.1 M$_\odot$/yr for Little Red Dots progenitors. Our models offer a metallicity-independent framework supporting quasi-stars as the source of Little Red Dot optical emission, and provide insights into their lifetimes, composition, and progenitor environment.

Key words. pending

1. Introduction

Since the recent discovery of so-called little red dots (LRDs; Matthee et al. 2024) their nature is being debated. While initially thought to be dusty active galactic nuclei (AGN) or massive galaxies (e.g. Kocevski et al. 2023; Labbé et al. 2023), the absence of classical AGN features, the finding of Balmer breaks exceeding predictions of standard stellar populations, and other characteristics, has led to alternative explanations invoking, for example, gas-enshrouded AGN (Inayoshi & Maiolino 2025), direct collapse black holes (DCBH; Pacucci et al. 2026), so-called BH stars (BH⋆s; Naidu et al. 2025; de Graaff et al. 2025), quasi-stars (QS; Begelman & Dexter 2026), primordial (PopIII) supermassive stars (SMS; Nandal & Loeb 2026), self-gravitating disks accreting onto SMS (Zwick et al. 2025), and tidal disruption events in runaway-collapsing clusters (Bellovary 2025).

While most of these explanations have in common the co-existence of a BH enshrouded by an optically thick gas envelope, several models are agnostic to their respective formation channel (e.g. the BH⋆ scenario), or the proposed formation and evolutionary scenarios differ significantly. Furthermore, DCBH and Pop III SMS models require metal-free gas conditions, which seem difficult to reconcile with the ubiquitous presence of metal-lines in LRDs (e.g. D'Eugenio et al. 2025; Pérez-González et al. 2026), although small amounts of metals could be produced shortly after the formation of the DCBH (e.g. Pacucci et al. 2026). It is therefore important to better understand the formation of these objects, and find metallicity-independent scenarios.

In this work we explore a metallicity independent scenario where initially low-mass protostars experience fast mass gain, e.g. from a net effect of mass loss and gain processes such as stellar winds, gas accretion, runaway stellar collisions in a dense and compact environment; leading to the formation of SMSs ($> 10^4$ M$_\odot$) consistent with the literature (e.g. Gieles et al. 2018; Ramírez-Galeano et al. 2025; Rantala et al. 2024). Subsequently, the SMS undergo the general-relativistic instability (GRI), leading to the formation of a central BH, becoming quasi-stars, i.e. objects in hydrostatic equilibrium with a central BH accreting the stellar envelope (Begelman et al. 2008). Several studies have shown that QS or SMS can reproduce several key observations features of LRDs (see Martins et al. 2020; Santarelli et al. 2026b; Begelman & Dexter 2026; Sneppen et al. 2026). Our model "unifies" SMS and QS scenarios for metal-free systems proposed earlier, generalizes them over a broad metallicity range, and proposes a consistent scenario for their formation and evolution, which enforces the possibility that LRDs host QSs.

2. Methods

To compute the formation and evolution of QS through rapid accretion onto initially low mass stellar objects, we use the MESA[1]

⋆ Corresponding author: jaime.romangarza@unige.ch

[1] The MESA release 25.10.1 is used for this work, as well as MESA SDK 24.7.1.

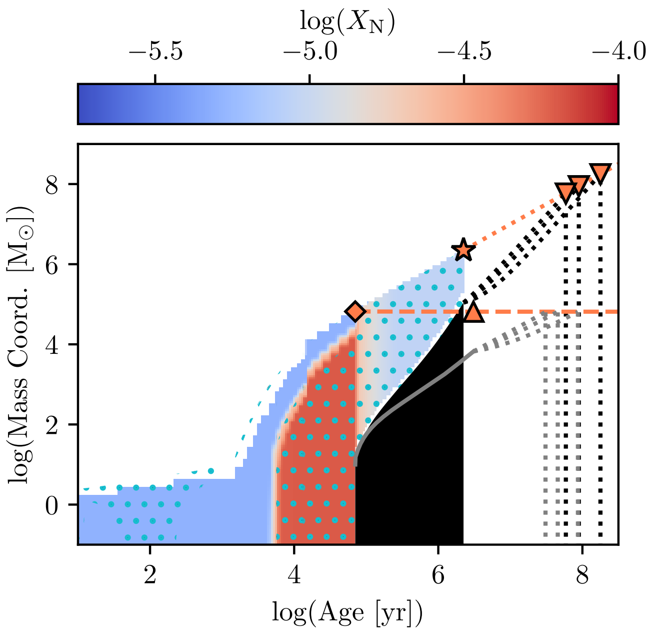

Fig. 1: Kippenhahn diagram showing the mass coordinate as a function of time for the model with $\dot{M}_{\rm gain,max}$ = 1 M$_\odot$/yr, $Z = 10^{-4}$ and $Y = 0.25$. The nitrogen mass fraction is color-coded; convection zones are indicated by cyan dots. The diamond shows the instant of GRI. The black filled region shows the BH mass. The non-accreting QS model is shown by the dashed orange line, and the corresponding BH mass by the solid grey line. The extrapolated QS mass for the accreting model is shown by the dotted orange line; that of the non-accreting model remains constant (orange dashed). The extrapolated BH masses are plotted with black and grey dotted lines, respectively; in each case, the three lines correspond to different estimates assuming $\alpha = 0.5$, 1, and 1.5. The star and the upward triangle indicate the crashing points of the accreting and non-accreting QS models. The downward triangles indicate the extrapolated masses of the object when the envelope has been entirely swallowed by the BH.

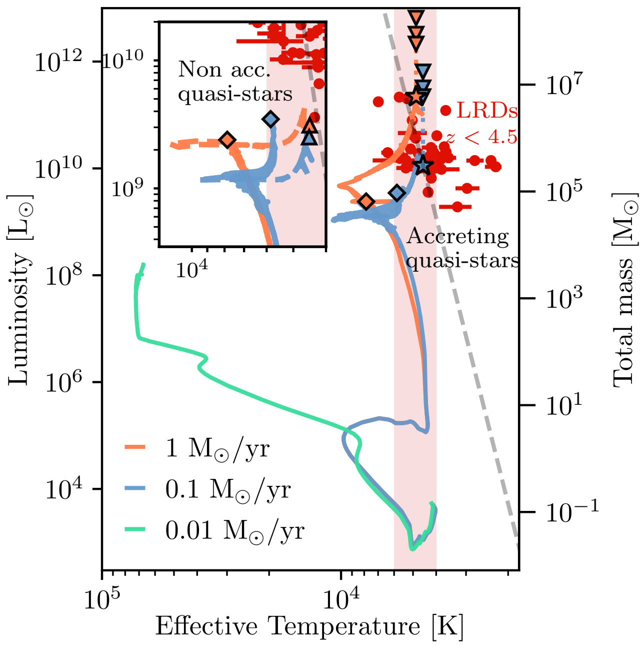

Fig. 2: Evolution in the HRD of the $Z = 10^{-4}$ models with the accretion rates color-coded. The approximate total mass of the star, or QS, is given by the right vertical axis (estimated by Eq. C.1). The solid lines represent the continuously accreting models. The non-accreting QSs are shown in dashed lines inside the nested plot. The diamonds, star, and triangles correspond to the same phases as in Fig. 1. The maximum values of the luminosity for the accreting QSs are estimated by the extrapolation of the QS mass and considering a constant $T_{\rm eff}$. The gray dashed line is a fit to the ending points of the QS models by Santarelli et al. (2026b). The red shaded region corresponds to the effective temperature range of the Hayashi line as considered by Inayoshi & Ho (2025). The observed LRD sample from de Graaff et al. (2025) is shown with red dots.

stellar evolution code (Paxton et al. 2010, 2013, 2015, 2018, 2019; Jermyn et al. 2023). All models start as a 2 M$_\odot$ proto-star with an initial radius of ∼ 200 R$_\odot$, constant entropy, and central temperature of ∼ 10^5 K. We compute models with metallicities $Z = 0$, 10^{-4}, 10^{-3} and 10^{-2} and helium mass fraction $Y = 0.25$, corresponding to [Fe/H]= $-\infty$, −2.10, −1.15 and −0.15 respectively. The models gain mass through cold accretion, while no explicit stellar wind prescription is considered. Initially, for numerical stability, we employ the variable accretion rate prescription by Haemmerlé et al. (2019), which depends on the bolometric luminosity, increased by hundredfold. Once the mass accretion rate has reached $\dot{M}_{\rm max,acc}$ = 0.01, 0.1 or 1 M$_\odot$/yr it is kept constant thereafter; this occurs while reaching masses from ∼ 10–10^3 M$_\odot$ depending on the threshold value. Details on the determining the GRI and other physical assumptions are described in Appendix A.

3. Results

3.1. Overview of the evolution from proto-star to quasi-star

The evolution of the accreting object through the proto-star, SMS, and QS phases of the model with the highest accretion rate ($\dot{M}_{\rm gain,max}$ = 1 M$_\odot$/yr) and $Z = 10^{-4}$ is shown in Fig. 1. After $t_{\rm GRI} \sim 7 \times 10^4$ yr and for a mass of $M_{\rm GRI} \sim 6.6 \times 10^4$ M$_\odot$ the object reaches the GRI and enters the QS phase. This occurs while the object is still burning hydrogen on the main sequence (the central He mass fraction has reached ∼ 0.30). The QS evolution then depends on the accretion rate of the central BH, $\dot{M}_{\rm BH}$, and on whether the QS continues to accrete material as $\dot{M}_{\rm BH}$ increases as the QS mass increases. In both cases, the simulations did not reach the point at which the stellar envelope is completely accreted by the BH, and we therefore analytically calculate the subsequent evolution, total lifetime, and final BH mass (see Appendix B).

The maximum mass the central BH can reach depends on the accretion history of the QS and the BH accretion rate. To extrapolate the BH mass after the `MESA` simulation encounters convergence problems and stops, and estimate the QS lifetime, we integrate Eq. B.2 over time, considering the values of the free parameter α = 0.5, 1 and 1.5 that accounts for possible enhancements or decrements of the BH accretion rate by, e.g., magnetic fields or angular momentum transport. Assuming $\dot{M}_{\rm gain,max}$ = 1 M$_\odot$/yr and that accretion is halted at the GRI, the estimated QS lifetime is $\lesssim 10^8$ yr, and the final mass of the QS therefore provides an upper limit to the final BH mass. In this case, the BH can reach a maximum mass of 6.6×10^4 M$_\odot$ by the end of the QS phase, that belongs in the intermediate mass range of BHs. If accretion onto the QS is maintained, the BH can grow up to ∼ 10^8 M$_\odot$ within

$\sim 10^8$ yr, given the adopted mass accretion rate. Note that the estimated QS lifetime is considered an upper limit, as our analytical results underestimate how $\dot{M}_{\rm BH}$ grows in time by comparing results from the simulations and the analytical formula. The different estimates given the value of α are also considered to explore this uncertainty.

For models with $\dot{M}_{\rm gain,max} = 0.1$ M$_\odot$/yr, the GRI occurs somewhat later ($t_{\rm GRI} \sim 0.36$ Myr) and at a lower mass ($M_{\rm GRI} \sim 3.6\times10^4$ M$_\odot$), but the total QS lifetime is similar to that of models with $\dot{M}_{\rm gain,max} = 1$ M$_\odot$/yr. The main estimation is that QSs are expected to last at most $\simeq 10^7$ to 10^8 yr (see Appendix B). For comparison, the lifetime of the non accreting QS models from Santarelli et al. (2026b) is estimated to be 30–40 Myr, that is consistent with our results. The expected lifetime of the QS progenitors depends on the mass gain rate but, as an order of magnitude approximation, it is 100–1000 times shorter than QS lifetime. For a more quantitative comparison between all QS models, see Appendix D and the table therein. Note also that the case with $\dot{M}_{\rm gain,max} = 0.01$ M$_\odot$/yr did not reach the GRI and was stopped earlier for numerical reasons.

The nucleosynthesis of rapidly accreting SMS and QS is also worth briefly discussing. As these objects burn H through the CNO cycle until the GRI is reached and remain essentially fully convective throughout, they can synthesize a maximum mass of Nitrogen $M_N = \overline{X_N} M_{\rm GRI} \leq X^{\rm ini}_{\rm CNO} M_{\rm GRI} \approx (1-1.5) \times 10^{-2}\, 10^{[{\rm O/H}]^{\rm ini}} M_{\rm GRI}$, where $\overline{X_N}$ is the average nitrogen mass fraction in the star and $X^{\rm ini}_{\rm CNO}$ the initial mass fraction in C+N+O. For the model shown in Fig. 1 with $[{\rm O/H}]^{\rm ini} = -2.1$, this corresponds to $M_N \approx (5-8)$ M$_\odot$, in agreement with the predicted average mass fraction $X_{\rm N} \sim 10^{-4}$ before the GRI is reached. No further nucleosynthesis occurs after that, during the QS phase, since temperature and density in the envelope are too low. If accretion continues beyond GRI, the N abundance rapidly decreases again to that of the accreted matter, as also shown in this figure. The surface abundances of these objects are therefore predicted to be variable with time but mostly determined by the accreting matter, and CNO equilibrium values (high N/O and N/C) can only be reached during a short amount of time or if the objects stop accretion close to or before GRI.

3.2. Evolution in the HR diagram

Figure 2 shows the evolutionary paths across the Hertzsprung-Russell diagram (HRD) of our models with $Z = 10^{-4}$. Starting from the lower-right corner of the HRD, the initial proto-star first contracts and moves towards higher effective temperatures and luminosities, exiting the domain defined by cool and fully convective stellar envelopes (i.e., 4000 K $\lesssim T_{\rm eff} \lesssim$ 6000 K), referred in the literature as the Hayashi line (see Hayashi 1961; Inayoshi & Ho 2025). When the luminosity reaches $\sim 3\times10^4$ L$_\odot$, the evolutionary tracks bifurcate. The model with $\dot{M}_{\rm gain,max} = 0.01$ M$_\odot$/yr departs towards higher effective temperatures (we remind that this model was computed up to a mass of $\simeq 4500$ M$_\odot$ and did not encounter the GRI). The other two models return towards the Hayashi line. This behavior is expected for accretion rates above ~ 0.02 M$_\odot$/yr, as extensively discussed in the literature (e.g., Haemmerlé et al. 2018; Herrington et al. 2023; Ramírez-Galeano et al. 2025; Nandal et al. 2023). Above this value, accretion causes the inflation of the stellar radius, as the timescale to radiate away the advected entropy becomes longer than the Kelvin-Helmholtz timescale. Consequently, models with $\dot{M}_{\rm gain,max} \gtrsim 0.1$ M$_\odot$/yr follow similar tracks, with the luminosity increasing at relatively low effective temperature as the stellar mass increases. Above 10^6 L$_\odot$, both stars gradually depart from the Hayashi line toward higher effective temperatures as they cease to be fully convective, returning once convection again dominates their structure.

The luminosity of SMSs is proportional to their mass and independent of the accretion rate (see Haemmerlé et al. 2018). Once the QS is formed, the luminosity of the remaining stellar envelope is regulated primarily by the QS total mass (central BH plus envelope), as previously found for metal-free QSs (e.g. Begelman et al. 2008; Santarelli et al. 2026b). The mass-luminosity relation from our models is shown in Appendix C.

The total stellar mass required to reach the GRI depends on the accretion rate (see Herrington et al. 2023; Nagele et al. 2022; Haemmerlé et al. 2018). Our models with $\dot{M}_{\rm gain,max} = 0.1$ and 1 M$_\odot$/yr reach it when they have masses $\gtrsim 3\times10^4$ M$_\odot$, consistent with values in the literature. At that instant they have a luminosity of $L_{\rm GRI}(\dot{M} \gtrsim 0.1\,{\rm M_\odot/yr}) \simeq 10^9$ L$_\odot$, and they become more luminous as the QS mass increases. For example, the model with $\dot{M}_{\rm gain,max} = 1$ M$_\odot$/yr reaches a total mass of $\sim 2.2\times10^6$ M$_\odot$ at the point the simulation stops due to convergence issues, corresponding to a luminosity of $\sim 2.2\times10^{11}$ L$_\odot$. If we extrapolate to the end of life of the QS, we find that it can reach a maximum luminosity of almost 10^{13} L$_\odot$ if it continues to grow in mass. In the case of non-accreting QS, our results are consistent with the models from Santarelli et al. (2026b). For a summary on the evolution in luminosity, effective temperature, stellar mass, and BH mass across different evolutionary epochs, see Appendix D and the table therein.

To study the effect of metallicity in our scenario we computed additional models with $\dot{M}_{\rm gain,max} = 1$ M$_\odot$/yr at $Z = 0$, 0.001 and 0.01. As shown in Fig. E.1, their evolution tracks are very similar, and they overlap remarkably during the QS phase. Also, the mass when GRI occurs, $M_{\rm GRI}$, increases only by a factor of two (from 46000 to 83000 M$_\odot$) from zero to solar metallicity. Nucleosynthesis depends on metallicity, but is largely determined by the composition of accreted matter (see above).

3.3. LRDs as QS hosts and implications on BH masses

In Fig. 2, we compare the predicted tracks of our SMS and QSs in the HR diagram with the LRD sample of de Graaff et al. (2025), for which bolometric luminosities and effective temperatures were obtained by fitting modified blackbody spectra to the rest-optical part of the observed spectra. The LRDs in this sample have luminosities $\sim 10^{9-11}$ L$_\odot$. Their inferred temperatures are comparable to those predicted by our models, especially if uncertainties in the effective temperature are considered (e.g. the efficiency of convection as shown in Santarelli et al. 2026b).

The comparison between the predicted and observed HRD and the position of these objects above $L > 10^9$ L$_\odot \sim L_{\rm GRI}$ may be explained by LRDs hosting QSs, which dominate their rest-optical emission. Furthermore, since the value of $L_{\rm GRI} \simeq 10^9$ L$_\odot$ depends on the accretion rate, it is also noted that QS progenitors should be formed through accretion rates $\gtrsim 0.1$ M$_\odot$/ year. Our results also imply that LRDs are intimately linked to BHs, as suggested by numerous earlier studies (e.g., Begelman & Dexter 2026; Ma et al. 2025; Greene et al. 2026). The corresponding bolometric luminosity provides a direct measure of the total mass of the QS, and hence an upper limit of the BH mass, since it represents an a priori unknown fraction of the QS mass. For example, predictions by Greene et al. (2026), based on the Eddington limit, may overestimate the BH mass up to two orders of magnitude.

Our scenario also predicts that objects with similarly low temperatures but luminosities $\lesssim L_{\rm GRI}$ should exist. One possibility is for them to be SMSs, but they should represent, as order of magnitude approximation, $\lesssim$ 0.1–0.01% of the overall population, since the stellar phase is $\sim$ 100 to $\sim$ 1000 times shorter than the lifetime in the QS phase, as discussed previously (cf. Appendix B). The other possibility evokes QSs whose progenitors accreted in a rate < 0.1 M$_\odot$/yr. The lack of LRDs with $L < 10^9$ L$_\odot$ may indicate that the progenitors of the inhabiting QSs had accretion histories of $\gtrsim 0.1$ M$_\odot$/yr.

Although we have not been able to compute consistent numerical models of QSs with masses well above 10^6 M$_\odot$, our analytical estimates show that such objects could grow up to masses of $\sim 10^8$ M$_\odot$ in case of continuing gas accretion with a rate of 1 M$_\odot$ yr^{-1} and be dominated by the BH mass (Fig. 1 and Table D.1). This would translate to luminosities up to $\simeq 10^{13}$ L$_\odot$, approximately a factor $\sim$ 10 times more luminous than the brightest LRD identified so far (see Ma et al. 2025). If nature indeed forms such objects and with the scenario indicated here remains to be seen.

4. Conclusions

As a pathway to understand the physical origin of the rest-optical emission from LRDs, we have calculated stellar evolution models of rapidly accreting stars. We start from low mass-proto-stars that experience a net mass gain and follow their evolution until they become SMS and reach the GRI, which leads to the formation of so-called QS (where a stellar envelope is supported by a central BH, see Begelman et al. 2006, 2008). We considered maximum mass gain rates of 0.001, 0.1 and 1 M$_\odot$/yr, and metallicities from $Z = 0$ to 0.01. We show that our scenario works independently of metallicity.

We are aware that the employed mass gain rates are in agreement with the mass-inflow rates onto simulated haloes from the cosmological simulations. For example, Cenci & Habouzit (2025) reports inflow rates range from $\sim 10^{-3}$ to $\gtrsim 1$ M$_\odot$/yr at $z \simeq 4$, which increase with higher redshifts. The mass growth threshold can also be reached in dense and compact forming massive star clusters with stellar surface densities similar to those estimated for LRDs (typically $> 10^5$ M$_\odot$ pc^{-2}), where both gas-accretion and collisions can concur to the formation of SMS, with no limitation in terms of metallicity, contrary to the DCBH scenarios (Gieles et al. 2018; Lahén et al. 2025; Baggen et al. 2026; Ramírez-Galeano et al. 2025, and references therein).

Accreting models with $\dot{M} \geq 0.01$ M$_\odot$/yr remain almost fully convective across the entire evolution, with effective temperatures from 4000 to 9000 K (consistent with Herrington et al. 2023; Haemmerlé et al. 2018; Nandal et al. 2023). Stars accreting at 0.1, 1 M$_\odot$/yr and $Z = 10^{-4}$ reach the GRI when they have masses of 3.5×10^4 M$_\odot$ and 6.6×10^4 M$_\odot$ respectively. Their luminosity at that instant is $\simeq 10^9$ L$_\odot$.

Significant amounts of material processed by the CNO cycle (N, in particular) can build up during the phase preceding the GRI. However, the continuing mass growth through the QS phase, which is needed to explain the observed luminosity range of LRDs, implies a strong dilution, and thus variable and not very strong chemical enrichment in QS.

The QS lifetime upper limit is estimated on the order of $10^7 - 10^8$ yr, consistent with the values the numerical models by Santarelli et al. (2026b). This is approximately 2-3 orders of magnitude longer than the lifetime of their stellar progenitors, depending as well on the progenitor's accretion history. Therefore, it is much more likely to observe QSs than their progenitors.

Our accreting QS models are in agreement with the effective temperatures and range of bolometric luminosities of observed LRDs, showing $L \sim 10^{9.5-11.5}$ L$_\odot$ (de Graaff et al. 2025). This suggests that LRDs may be dominated by QSs with total masses between $\sim 10^{4.5-6.5}$ M$_\odot$. The mass of their central BH depends on the evolutionary stage of the QS and its accretion history, and the QS mass serves only as its upper limit. Assuming that the QS mass is of the same order as the BH mass (as in Greene et al. 2026) may overestimate the value of the latter.

From our models, the minimum bolometric luminosity of $\simeq 10^9$ L$_\odot$ of LRDs implies that the QS progenitors should have a minimum accretion rate of $\simeq 0.1$ M$_\odot$/yr. If such minimum observed luminosity was higher it would imply that the minimum accretion rate of the QS progenitors is > 0.1 M$_\odot$/yr and vice versa. The accreting QS scenario does not place a limit on its maximum luminosity, but such quantity provides context on the maximum amount of mass that these objects can reach while comparing them with LRD observations.

Acknowledgements. This work was supported by the Swiss National Science Foundation (PI Fragos, project number CRSII5_213497). The authors thank M. Habouzit for the discussions regarding this work. This work has received funding from the Swiss State Secretariat for Education, Research and Innovation under contract number MB22.00072, as well as from the Swiss National Science Foundation through project grant 200020_207349. The Cosmic Dawn Center is funded by the Danish National Research Foundation under grant DNRF140.

References

Baggen, J. F. W., Scoggins, M. T., van Dokkum, P., et al. 2026, arXiv e-prints, arXiv:2602.02702
Ball, W. H. 2012, arXiv preprint arXiv:1207.5972
Begelman, M. C. & Dexter, J. 2026, ApJ, 996, 48
Begelman, M. C., Rossi, E. M., & Armitage, P. J. 2008, MNRAS, 387, 1649
Begelman, M. C., Volonteri, M., & Rees, M. J. 2006, MNRAS, 370, 289
Bellovary, J. 2025, ApJ, 984, L55
Cenci, E. & Habouzit, M. 2025, MNRAS, 542, 2597
de Graaff, A., Hviding, R. E., Naidu, R. P., et al. 2025, arXiv e-prints, arXiv:2511.21820
D'Eugenio, F., Nelson, E., Ji, X., et al. 2025, arXiv e-prints, arXiv:2510.00101
Gieles, M., Charbonnel, C., Krause, M. G. H., et al. 2018, MNRAS, 478, 2461
Greene, J. E., Setton, D. J., Furtak, L. J., et al. 2026, ApJ, 996, 129
Haemmerlé, L., Eggenberger, P., Ekström, S., et al. 2019, A&A, 624, A137
Haemmerlé, L., Woods, T. E., Klessen, R. S., Heger, A., & Whalen, D. J. 2018, MNRAS, 474, 2757
Hayashi, C. 1961, Publications of the Astronomical Society of Japan, 13, 450
Herrington, N. P., Whalen, D. J., & Woods, T. E. 2023, MNRAS, 521, 463
Inayoshi, K. & Ho, L. C. 2025, arXiv preprint arXiv:2512.03130
Inayoshi, K. & Maiolino, R. 2025, ApJ, 980, L27
Jermyn, A. S., Bauer, E. B., Schwab, J., et al. 2023, ApJ Supplement Series, 265, 15
Kocevski, D. D., Onoue, M., Inayoshi, K., et al. 2023, ApJ, 954, L4
Labbé, I., van Dokkum, P., Nelson, E., et al. 2023, Nature, 616, 266
Lahén, N., Naab, T., Rantala, A., & Partmann, C. 2025, MNRAS, 543, 1023
Loeb, A. & Rasio, F. A. 1994, arXiv preprint astro-ph/9401026
Ma, Y., Greene, J. E., Volonteri, M., et al. 2025, arXiv e-prints, arXiv:2509.02662
Martins, F., Schaerer, D., Haemmerlé, L., & Charbonnel, C. 2020, A&A, 633, A9
Matthee, J., Naidu, R. P., Brammer, G., et al. 2024, ApJ, 963, 129
Nagele, C., Umeda, H., Takahashi, K., Yoshida, T., & Sumiyoshi, K. 2022, MNRAS, 517, 1584
Naidu, R. P., Matthee, J., Katz, H., et al. 2025, arXiv preprint arXiv:2503.16596
Nandal, D. & Loeb, A. 2026, ApJ, 998, 124
Nandal, D., Regan, J. A., Woods, T. E., et al. 2023, A&A, 677, A155
Pacucci, F., Ferrara, A., & Kocevski, D. D. 2026, arXiv e-prints, arXiv:2601.14368
Paxton, B., Bildsten, L., Dotter, A., et al. 2010, ApJ Supplement Series, 192, 3
Paxton, B., Cantiello, M., Arras, P., et al. 2013, ApJ Supplement Series, 208, 4
Paxton, B., Marchant, P., Schwab, J., et al. 2015, ApJ Supplement Series, 220, 15
Paxton, B., Schwab, J., Bauer, E. B., et al. 2018, ApJ Supplement Series, 234, 34
Paxton, B., Smolec, R., Schwab, J., et al. 2019, ApJ Supplement Series, 243, 10
Pérez-González, P. G., Barro, G., Carniani, S., et al. 2026, arXiv e-prints, arXiv:2602.20247
Ramírez-Galeano, L., Charbonnel, C., Fragos, T., et al. 2025, A&A, 699, A223
Rantala, A., Naab, T., & Lahén, N. 2024, MNRAS, 531, 3770
Santarelli, A. D., Campbell, C. B., Farag, E., et al. 2026a, ApJ, 998, 150
Santarelli, A. D., Farag, E., Bellinger, E. P., et al. 2026b, ApJ Letters, 998, L4
Sneppen, A., Watson, D., Matthews, J. H., et al. 2026, arXiv e-prints, arXiv:2601.18864
Volonteri, M. & Rees, M. J. 2005, ApJ, 633, 624
Zwick, L., Tiede, C., & Mayer, L. 2025, arXiv e-prints, arXiv:2507.22014

Appendix A: Physical assumptions

To account for general relativistic effects, the gravitational constant is modified according to the first order correction given by the Tolman–Oppenheimer–Volkoff equation, which is derived for the Schwarzschild metric. The correction is computed as (e.g. see Herrington et al. 2023):

$$G_{\rm TOV} = G\left(1 + \frac{P}{\rho c^2} + \frac{4\pi P r^3}{m_r c^2}\right)\left(1 - \frac{2Gm_r}{rc^2}\right)^{-1}. \tag{A.1}$$

The evolution of the stars stops when the general-relativistic instability (GRI) criterion by Nagele et al. (2022) is reached:

$$\Gamma_1(m_r) < \frac{4}{3} + 4.498\frac{G_{\rm TOV} m_r}{rc^2} f_{\rm GR}. \tag{A.2}$$

$\Gamma_1(m_r)$ corresponds to the value of the adiabatic index at the mass coordinate m_r , which corresponds to the radial coordinate r. The factor $f_{\rm GR}$ is introduced and chosen as 1.5 to stop the evolution of the stellar models before they reach the GRI and become numerically unstable. The models stop when they have $\gtrsim 70\%$ of the stellar mass needed to reach the GRI given $f_{\rm GR} = 1$.

When the GRI is encountered (i.e., Eq. A.2 is satisfied) the stellar evolution run is halted. The core of the corresponding supermassive star is expected to collapse into a BH (Loeb & Rasio 1994; Volonteri & Rees 2005; Begelman et al. 2006). It then enters a new evolutionary phase as a QS (Begelman et al. 2008), where the system is stabilized against gravity primarily by the radiation produced from accretion onto the central BH. Stars that encounter the GRI after the main sequence may experience the general relativistic instability supernova (GRISN) where no black BH is expected to be formed (see Nagele et al. 2022; Haemmerlé et al. 2018). For this work we do not explore the cases where the GRISN is triggered.

The evolution of the QS model is computed with the `MESA-QUEST` module (see Santarelli et al. 2026a). We investigate two limiting cases, one where gas accretion stops as soon as the GRI is encountered, and one where accretion onto the QS continues at the same rate as previously. In both cases, the central boundary condition of the model is set to an initial BH mass of 10 $M_\odot$. The central BH grows in mass through the accretion of the stellar envelope following the convection-limited Bondi accretion rate (Ball 2012), with both convective and radiative efficiencies both set to 0.1. The BH accretion luminosity is set in terms of the radiative efficiency and accretion rate as $\simeq 0.11\, \dot{M}_{\rm acc}\, c^2$ (see Santarelli et al. 2026a).

Appendix B: Lifetime of quasi-stars

The aim of this section is provide an analytical prediction for the lifetime of QSs depending on the accretion history during this phase. We define that the QS progenitors have a constant mass gain rate $\dot{M}$, therefore their mass across time is modeled as

$$M(t) = \dot{M}\, t, \quad \text{if } t < t_{\rm GRI}. \tag{B.1}$$

Where $t_{\rm GRI}$ is the instant the GRI is encountered, its exact value depends on the accretion rate, e.g., for an accretion rate of 0.1 $M_\odot$/yr it can be estimated as $t_{\rm GRI} \simeq 10^{4.5} M_\odot/\dot{M}$ (see Herrington et al. 2023).

After $t_{\rm GRI}$ the central BH is formed with an initial mass of $M_{\rm BH,i}$. The BH accretion, $\dot{M}_{\rm BH}$, rate can also be written as a function of the QS mass, following of Santarelli et al. (2026b):

$$\dot{M}_{\rm BH} = \frac{1-\epsilon}{\epsilon}\frac{4\pi}{\kappa c}\,\alpha\, G_{\rm TOV}\, M\,, \tag{B.2}$$

where $\epsilon = 0.1$ is the radiative efficiency, κ is the opacity of the material surrounding the BH and set at the inner boundary of the model, M is the total mass of the QS. The free parameter α is used to account for possible decreases or enhancements in $\dot{M}_{\rm BH}$ due to angular momentum transport or magnetic fields, respectively.

For the QS we consider two cases: either the QS continues to accrete at the same rate as its progenitor, or it stops accreting completely. We define the end of the QS phase as the instant the central BH has accreted the remaining stellar envelope, i.e. $M_{\rm BH} = M$.

The mass of the BH grows following Eq. B.2,

$$\dot{M}_{\rm BH} = \begin{cases} \frac{2}{\tau'}\, M(t_{\rm GRI}) & \text{if } \dot{M} = 0, \\ \frac{2}{\tau'}\, \dot{M}\, t & \text{if } \dot{M} > 0. \end{cases} \tag{B.3}$$

Where $\tau' = \left(\frac{1-\epsilon}{\epsilon}\frac{2\pi}{\kappa c}\,\alpha\, G\right)^{-1}$, this quantity has units of time.

After integrating over time from $t_{\rm GRI}$ until the end of the QS phase, i.e. $t_{\rm end}$, we find that the BH mass is

$$M_{\rm BH} = \begin{cases} M_{\rm BH,i} + \frac{2}{\tau'}\, M(t_{\rm GRI})\,(t_{\rm end} - t_{\rm GRI}) & \text{if } \dot{M} = 0, \\ M_{\rm BH,i} + \frac{1}{\tau'}\, \dot{M}\,(t_{\rm end} - t_{\rm GRI})^2 & \text{if } \dot{M} > 0. \end{cases} \tag{B.4}$$

At $t_{\rm end}$ we have $M_{\rm BH}/M = 1$. In the case where $\dot{M} = 0$ we obtain the following asymptotic behavior for $t_{\rm end}$:

$$t_{\rm end,no\ acc} \sim \begin{cases} \tau'/2 & \text{if } t_{\rm GRI} \ll \tau', \\ 3\tau'/2 & \text{if } t_{\rm GRI} \to \tau', \\ t_{\rm GRI} & \text{if } \tau' \ll t_{\rm GRI}. \end{cases} \tag{B.5}$$

For the case where the QS keeps accreting, its lifetime is determined as:

$$t_{\rm end,acc} \sim \begin{cases} \tau' & \text{if } t_{\rm GRI} \ll \tau', \\ \frac{3+\sqrt{5}}{2}\,\tau' & \text{if } t_{\rm GRI} \to \tau', \\ t_{\rm GRI} + \sqrt{t_{\rm GRI}\,\tau'} & \text{if } \tau' \ll t_{\rm GRI}. \end{cases} \tag{B.6}$$

In all cases $t_{\rm end,acc} > t_{\rm end,no\ acc}$, and

$$\frac{t_{\rm end,acc}}{t_{\rm end,no\ acc}} \sim \begin{cases} 2 & \text{if } t_{\rm GRI} \ll \tau', \\ 1 & \text{if } \tau' \ll t_{\rm GRI}. \end{cases} \tag{B.7}$$

As the lifetime of QSs depends mainly on τ', we estimate its value as it depends only on ϵ, α and κ. If $\epsilon = 0.1$, $\alpha = 1$ and $\kappa = 0.38$ cm^2/g (this value is extracted from our simulations and is mostly constant during the QS phase), one obtains $\tau' \simeq 10^8$ yr. This value is consistent with the estimates from our simulations. Also, in Appendix D one can notice that the estimated lifetime of the accreting QSs is approximately twice as the non-accreting ones, consistent with Eq. B.7.

Lastly, we compare the the lifetime of the QS progenitor to the duration of the QS phase as

$$\frac{t_{\rm QS\ prog.}}{t_{\rm QS}} = \frac{t_{\rm GRI}}{t_{\rm end} - t_{\rm GRI}}. \tag{B.8}$$

For an accretion rate of 0.1 $M_\odot$/yr it corresponds to $t_{\rm GRI} \sim 10^5$ yr. As $t_{\rm end} \sim 10^8$ yr, then we estimate, for this particular case, that the QS phase lasts one thousand times more than the life of its progenitor. If the accretion rate increases, then $t_{\rm GRI}$ decreases and vice versa (see Herrington et al. 2023), while $t_{\rm end}$ remains mostly constant.

It is important to note that the estimate for $t_{\rm end}$ should be considered an upper value for the QS lifetime. Compared with our simulations, the value of $\dot{M}_{\rm BH}$ is higher than the one obtained from Eq. B.2, which being more consistent with $\alpha > 1$.

Appendix C: Mass-luminosity relation

Fig. C.1 show the mass-luminosity relation for the continuously accreting models. For stars with masses $\gtrsim$ 100 $M_\odot$ the relation is independent of the accretion rate and metallicity (see e.g. Martins et al. 2020), and it essentially follows the Eddington luminosity of the object,

$$L_{\rm Edd} = \frac{4\pi G m_p c}{\sigma_T} M = 3.7 \times 10^4 L_\odot \left(\frac{M}{M_\odot}\right). \quad \text{(C.1)}$$

For accretion rates between 0.1 to 1 $M_\odot$/yr, the stars will encounter the GRI when they reach masses between $\sim 10^{4.5}$ to $\sim 10^{5.5}$ $M_\odot$, and it is expected that they will be in the MS at that point (Herrington et al. 2023; Nagele et al. 2022; Haemmerlé et al. 2018). Once the QS phase begins the relation between mass and luminosity stays similar to the one in the stellar phase (e.g., Santarelli et al. 2026b).

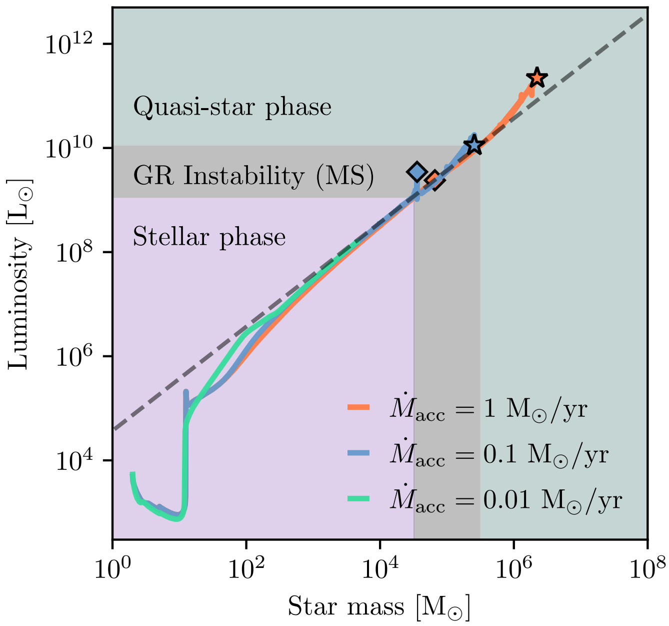

Fig. C.1: Luminosity as a function of stellar mass for the continuously accreting models: 1 $M_\odot$/yr (orange), 0.1 $M_\odot$/yr (blue), and 0.01 $M_\odot$/yr (mint). The instant when the GRI criterion is met is marked by diamond symbols in the corresponding colours. The grey shaded region denotes the mass range where the GRI is expected to occur, for main-sequence stars with accretion rates from 0.1 to 1 $M_\odot$/yr (see Haemmerlé et al. 2018; Nagele et al. 2022; Herrington et al. 2023), and their corresponding luminosities. The black dashed line represents the mass–luminosity relation obtained by setting the stellar luminosity equal to the Eddington luminosity.

Appendix D: Mass, luminosity and effective temperature across the stellar evolution and QS phases

Table D.1 shows the evolution of stellar mass, luminosity, effective temperature and BH mass for three different epochs of the models' evolution, in the cases where the QS keeps accreting mass or not. First, such quantities are reported for the instant when the GRI condition is met, at that time the BH mass is zero. The second epoch corresponds to the point when the simulations crash. The last section shown the extrapolated values for the end of life of the QS and the resulting BH mass for different values of the parameter α from Eq. B.2.

Appendix E: Evolutionary tracks of QSs for different metallicities

Fig. E.1 shows the HRD for models with $\dot{M}_{\rm gain,max}$ = 1 $M_\odot$/yr and metallicities from Z = 0 to 0.1. The models evolution across metallicities remain similar, allowing to present the accreting QS scenario as independent of metallicity in the context of LRDs.

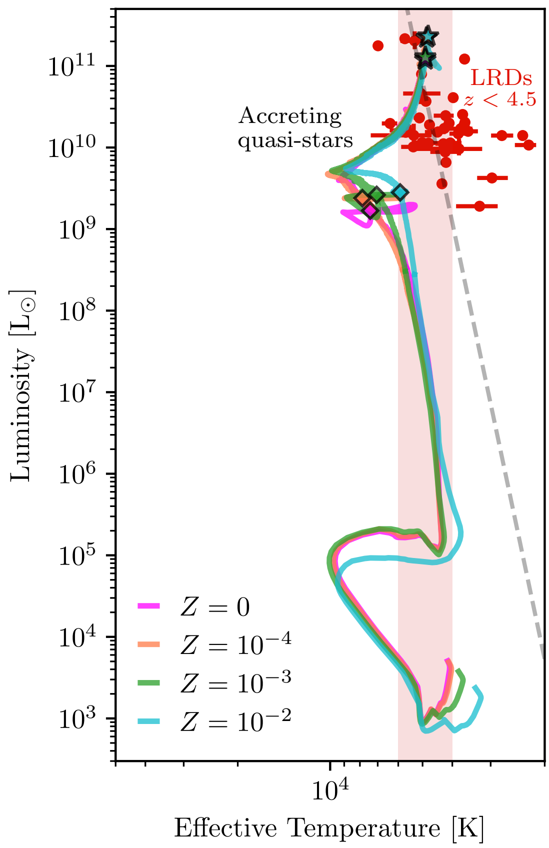

Fig. E.1: Similar to Fig. 2, showing accreting models with $\dot{M}_{\rm gain,max}$ = 1 $M_\odot$/yr and different metallicities color-coded.

Table D.1: Relevant quantities for the models with maximum mass gain rates $\dot{M}_{\rm gain,max}$ = 0.1 and 1 $\mathrm{M}_\odot$/yr, Y = 0.25 and $Z = 10^{-4}$.

$\dot{M}_{\rm gain,max}$	Acc. QS	$t_{\rm GRI}$	$M_{\rm GRI}$	$L_{\rm GRI}$	$T_{\rm eff,GRI}$	$t_{\rm crash}$	$M_{\rm crash}$	$L_{\rm crash}$	$T_{\rm eff,crash}$	$M_{\rm BH,crash}$		$t_{\rm end,extrap}$ [Myr]			$M_{\rm BH,extrap}$ [10^6 $\mathrm{M}_\odot$]		
[$\mathrm{M}_\odot$/yr]		[Myr]	[10^6 $\mathrm{M}_\odot$]	[10^9 $\mathrm{L}_\odot$]	[K]	[Myr]	[10^6 $\mathrm{M}_\odot$]	[10^9 $\mathrm{L}_\odot$]	[K]	[$\mathrm{M}_\odot$]	α =	0.5	1	1.5	0.5	1	1.5
0.1	Yes	0.359	0.036	3.473	5838	2.218	0.256	11.255	4542	10174		177.637	89.029	60.191	17.392	8.737	5.985
0.1	No	0.359	0.036	3.473	5838	2.915	0.035	2.513	4486	3176		87.875	45.068	31.179	0.036	0.036	0.036
1	Yes	0.07	0.066	2.396	7850	2.24	2.224	221.088	4854	109639		177.955	89.189	58.927	175.975	88.403	57.864
1	No	0.07	0.066	2.396	7850	2.376	0.655	3.11	4471	4764		86.665	45.483	30.75	0.066	0.066	0.066